We are IntechOpen, the world's leading publisher of Open Access books Built by scientists, for scientists

6,900
Open access books available

185,000
International authors and editors

200M
Downloads

Our authors are among the

154
Countries delivered to

TOP 1%
most cited scientists

12.2%
Contributors from top 500 universities



WEB OF SCIENCE™

Selection of our books indexed in the Book Citation Index in Web of Science™ Core Collection (BKCI)

Interested in publishing with us?
Contact book.department@intechopen.com

Numbers displayed above are based on latest data collected.
For more information visit www.intechopen.com



Chapter 6

Single-Walled Carbon Nanohorn (SWNH) Aggregates Inhibited Proliferation of Human Liver Cell Lines and Promoted Apoptosis, Especially for Hepatoma Cell Lines

Guoan Xiang, Jinqian Zhang and Rui Huang

Additional information is available at the end of the chapter

http://dx.doi.org/10.5772/61109

Abstract

Research focus: SWNHs (single-walled carbon nanohorns) may be utilized to treat cancer as drug carriers based on their particular structure. But, the effect mechanism of the material itself on liver cells has not been investigated. **Research methods used**: To answer those questions, the roles of rude SWNHs on the biology functions of human liver normal and cancer cells were studied. **Results/findings of the research**: The results indicated that SWNHs suppressed growth, proliferation, and mitotic entry of human liver normal and cancer cells, and also pushed cell apoptosis, especially in cancer cells. We had found SWNHs in the lysosomes of L02 cells and in the nuclei of HepG2 cells. It indicated that individual spherical SWNH particles could enter into liver cells. **Main conclusions and recommendations**: Our results identified that it had different mechanisms between SWNHs and hepatoma cell lines or human normal cell lines. Advanced research about application and mechanisms in the treatment of HCC (hepatocellular carcinoma) by SWNHs should be carried out.

Keywords: SWNHs (single-walled carbon nanohorns), hepatocellular carcinoma, apoptosis, proliferation

1. Introduction

SWNHs (single-walled carbon nanohorns) were first synthesized by Iijima et al. [1] in 1999. On the basis of their special surface structures and large surface areas, SWNHs may be used

INTECH
open science | open minds

© 2015 The Author(s). Licensee InTech. This chapter is distributed under the terms of the Creative Commons Attribution License (http://creativecommons.org/licenses/by/3.0), which permits unrestricted use, distribution, and reproduction in any medium, provided the original work is properly cited.

in pharmacy and biomedicine. [2, 8] Some investigators [4] have applied oxidized SWNHs (SWNHox) as drug carriers with cisplatin for treatment of cancer. They found that SWNHs could slowly release cisplatin and inhibit effectively the proliferation of human lung cancer cells NCI-H460.

The results from their research also demonstrated that SWNHox itself could not suppress or promote the proliferation of human cancer cells as carrier material. In addition, up to now, the functions of unembellished SWNHs on cells were not very apparent. [9] Many researchers have studied the biological functions of graphene, fullerene, and carbon nanotubes (CNTs). [10, 32] They found that nanoparticles of carbon could enter into cells, even subcellular organelles such as lysosomes or nuclei. [17, 21, 23, 24] Carbon nanoparticles can induce apoptosis related to oxidative stress. [33, 36]

How SWNHs influence the functions of L02 (human normal liver cell lines) and HepG2 (human hepatoma cell lines) was unknown. Moreover, the differences role mechanisms between the material and normal liver cells or cancer liver cells had not been studied. To answer these questions, the direct effects of SWNHs on human hepatoma cell line HepG2 and human liver normal cell line L02 were investigated. We performed internalization in liver cell lines with SWNH particles. The extraordinarily different role induced by SWNHs on hepatoma cell lines and liver normal cell lines, will be useful for the treatment of HCC (hepatocellular carcinoma). To understand how studies on nanomaterial toxicology might relate to nanomedicine safety, it is important to consider the current regulatory framework (legally binding requirements and guidelines) in place for all medicine evaluations.

2. Characterization of material

By arc-discharge method, SWNHs was synthesized in air. It's characterized by high-resolution transmission electron microscopy (HRTEM), Raman spectra, and thermogravimetry, as previously reported [37]. SWNHs are dahlia-like structures and spherical aggregates; the diameters of SWNHs ranged from 60–100 nm. We determined other elemental contents of SWNHs with S4 Explorer X-ray fluorescence spectrometer. We detected the elemental contents of SWNHs with rapid N tube.

2.1. Preparation of dishes coated with SWNHs

SWNHs were suspended in ultrapure dialysis water from Milli-Q Integral Water 5 Purification System. SWNHs solution (10 μg/mL) were placed on PS (polystyrene) dishes and dried at 80°C in air for 4 h. Then these dishes were treated with ultraviolet irradiation for 1 h. The abbreviations SWNHs10, SWNHs20, SWNHs30, and SWNHs40 correspond to 0.21 μg/cm^2, 0.42 μg/cm^2, 0.64 μg/cm^2, and 0.85μg/cm^2 in each dish (60 mm), respectively. [24] Dataphysics OCA 40 Contact Angle Measuring System was used to determine the contact angles of 2 μl volume water droplets on the noncoated PS surfaces and the SWNHs40-coated surfaces at 20°C.

http://dx.doi.org/10.5772/61109

2.2. Cell culture

HepG2 and L02 cells were seeded onto noncoated PS dishes and dishes were coated with SWNHs10, SWNHs20, SWNHs30, SWNHs40, and then cultured with DMEM (Dulbecco's Modified Eagle's Medium supplemented), 1% penicillin-streptomycin solution, and 10% fetal bovine serum at 37°C in 5% CO_2. [24]

2.3. Growth curve and morphology of liver cells cultured with SWNHs

HepG2 (3×10^5) and L02 (3×10^5) cells were seeded onto dishes, respectively. After being cultured for 48 h, these cells were subsequently visualized with optical microscope, based on the general protocol. These cells were observed and photos were acquired with a camera. At 48 h, cells were numbered with cell counter plate. The polynomial fitting about relationship between quantities (μg) of SWNHs (NH) and number of cells (CN) was carried out with using Origin 8 software.

2.4. Measurement of mitotic entry

These cells were synchronized with thymidine and cultured on dishes coated with SWNHs for 16 h. Then the cells were released into cell cycle with fresh medium. In the end, these cells were gathered or treated at different time points for subsequent specific analyses. DNA synthesis was measured with bromodeoxyuridine (BrdU) labeling in these cells. The BrdU-positive and the total number of cells were counted. Mitotic cells were evaluated by time-lapse videomicroscopy with Openlab software. [38]

2.5. Assessment of SWNHs

Elemental composition of SWNHs included 0.25% total metal content and 95.3% carbon, each metal less than 0.1%. [39, 41] Our results indicated that the surface area of BET was 631.55m^2/g. [42] The results with regard to adsorptive isotherm plot of SWNHs showed that the surface of SWNHs particles was hydrophobic.

At the relative pressure 0.994 (P/P_o), the diameter of SWNHs material was less than 308.7 nm. Moreover, the pore volume of SWNHs was 1.57 cm^3/g. The average pore diameter of SWNHs was 9.97 nm. The particle density was 1.0077 g/cm^3. The pore size distribution by Barrett-Joyner-Halenda (BJH) indicated that diameters of most mesopores were 2–8 nm in the SWNHs material. These results showed that SWNHs had many closed pores. The dimension range of suspended SWNHs particle was 295–615 nm in aqueous solution.

2.6. Characterization of dishes coated with SWNHs

Single particles of SWNHs on the surface of dishes were showed in images from scanning electron microscope (SEM); their diameters were 60–100 nm (Figure 1). The aggregates of secondary SWNH were dispersed and exhibited on individual particles on the surface of PS dishes. On surface of PS dishes, the contact angle of water droplet was 44.9°, less than the dried

SWNHs-coated surface at 74.5°. The hydrophobicity of uncoated PS surface was lower than that of SWNHs40/PS surface.

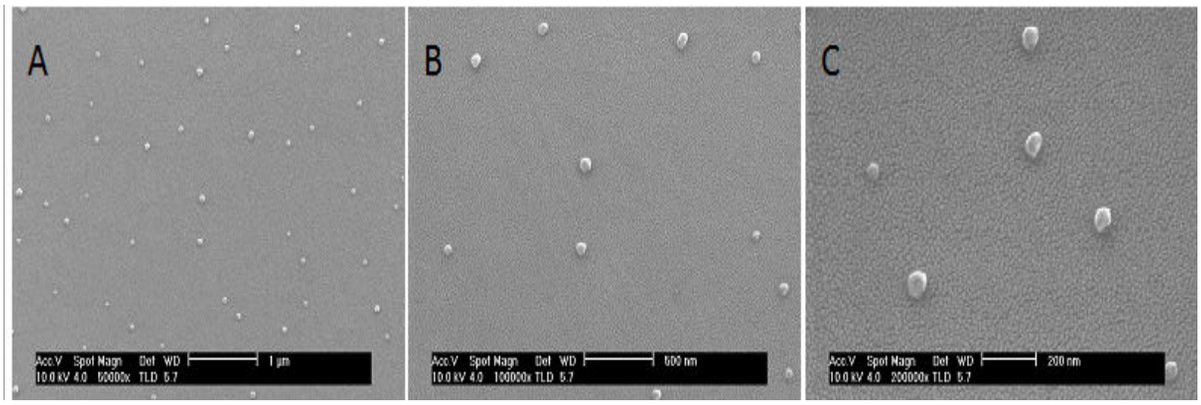


Figure 1. The films of SWNHs40/PS observed by SEM. SWNHs40-coated PS (0.85 μg/cm^2) dishes with a bottom area of about 1 cm^2 were prepared for SEM measurements. After pretreated by spraying gold on films of samples, SEM measurements were carried out using a SIRION field emission scanning electronic microscope (FEI Corporation Ltd) with accelerating voltage of 10.0kV. The SEM of films showed that SWNHs40 on PS surface (0.85 μg/cm^2) were individual spherical particles with diameters of 60-100nm. (A) 50,000×, scale bar represents 1μm. (B) 100,000×, scale bar represents 500 nm. (C) 200,000×, scale bar represents 200nm.

2.7. Morphology of cells

The morphology of cells cultured for 48 h in SWNH-coated and uncoated dishes was observed by optical microscope. The images showed that the number of L02 (Figure 2 A–C) and HepG2 (Figure 2 D–F) decreased in a concentration-dependent manner. More spherical cells could be observed, which became smaller in size. That was remarkable in HepG2 cells. SWNHs had a much larger effect on liver cancer cells than normal as proliferation inhibitor factor.

2.8. SWNHs inhibit mitotic entry, proliferation, and growth of liver cells

With increased quantities of SWNHs, the growth curves of HepG2 and L02 cells are shown at 48 h; both the amounts of L02 (Figure 2G, lower curve) and HepG2 (Figure 2H, upper curve) decreased noticeably in a concentration-dependent manner (P<0.01). In addition, polynomial fitting with regard to relationships between NH and CN was carried out. The proliferate rate of HepG2 was faster than L02 cells, but follow with the increase of NH, proliferation of HepG2 was remarkably shut down and gradually approached to L02 cells. The polynomial fitting formula of L02 (lower dotted curve, Figure 2G) was as follows:

$$\left[CN\right] = -26.2\left[NH\right]^4 + 1.23\times10^3\left[NH\right]^3 - 1.29\times10^4\left[NH\right]^2 - 1.20\times105\left[NH\right] + 1.96\times10^6,\ R2=1. \quad (1)$$

The polynomial fitting formula of HepG2 (upper dotted curve, Figure 2G) was as follows:

$$\left[CN\right] = -1.46\times10^2\left[NH\right]^4 + 7.42\times10^3\left[NH\right]^3 - 1.19\times10^5\left[NH\right]^2 + 4.56\times10^5\left[NH\right] + 4.33\times10^6,\ R2=1. \quad (2)$$

http://dx.doi.org/10.5772/61109

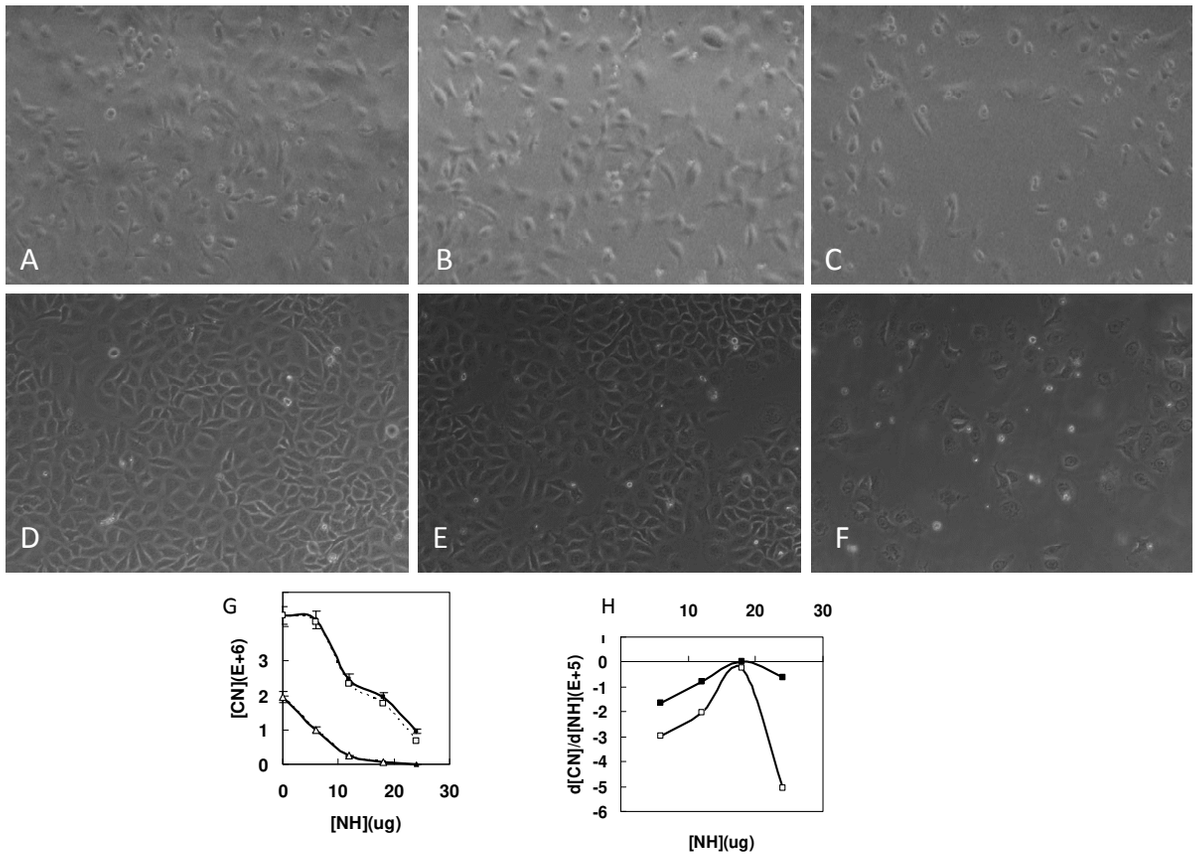


Figure 2. Morphology observed by optical microscope and growth curves of L02 and HepG2 cells cultured onto non- and SWNHs-coated dishes. L02 (3×10^5) and HepG2 (3×10^5) cells were seeded onto 60-mm non- and SWNHs-coated dishes and cultured for 48 h, and then images of the cells were observed according to the general protocol by optical microscope and total numbers of L02 and HepG2 cells [CN] were counted, respectively. The cells were visualized and digital images were acquired using Nikon camera (Nikon, Japan). Fig. 2G are cell growth curves of L02 (Fig. 2G Lower curve) and HepG2 (Fig. 2G Upper curve) ($P<0.01$). All data are represented as mean ±SEM. The polynomial fitting formulas for the relationship between cell number [CN] and quantity of SWNHs (μg) [NH] was performed by Origin 8 (Fig. 2G Dotted curves). Fig. 2H are the first-order derivates *d [CN]/d [NH]* deduced from the two polynomial fitting formulas (A) Control, L02 untreated with SWNHs; (B) L02 treated with SWNHs20 (0.42ìg/cm^2); (C) L02 treated with SWNHs40 (0.85ìg/cm^2) (400×); (D) Control, HepG2 untreated with SWNHs; (E) HepG2 treated with SWNHs20 (0.42ìg/cm^2); (F) HepG2 treated with SWNHs40 (0.85ìg/cm^2) (400×); (G) Lower curve: —▲—L02 determined, ---△--polynomial fitting L02 Upper curve: —■—HepG2 determined, ---□-- polynomial fitting HepG2 (H) Lower curve: —□— The first-order derivate d [CN]/d [NH] of HepG2 Upper curve: ---■--The first-order derivate d [CN]/d [NH] of L02

Both the relationships between the number of L02 or HepG2 cells and the quantities of SWNHs are quartic polynomial.

The first-order derivates of the above two formulas (d [CN]/d [NH]) were also deduced. The first-order derivate of L02 (upper curve, Figure 2H) was as follows:

$$d\left[CN\right]/d\left[NH\right] = -1.048\times10^{2}\left[NH\right]^{3} + 3.69\times10^{3}\left[NH\right]^{2} - 2.58\times10^{4}\left[NH\right] - 1.20\times10^{5} \quad (3)$$

The first-order derivate of HepG2 (lower curve, Figure 2H) was as follows:

$$d\left[CN\right]/d\left[NH\right] = -5.84\times10^{2}\left[NH\right]^{3} + 2.23\times10^{4}\left[NH\right]^{2} - 2.38\times10^{5}\left[NH\right] + 4.56\times10^{5} \quad (4)$$

First-order derivative denoted that the changed rate of cell numbers followed with the increasing concentration of SWNHs. The formula of the changed rate was negative value, which suggested that SWNHs suppressed proliferation of liver cells. Moreover, the low changed rate of HepG2 cells compared to L02 cells revealed the more obvious inhibitory effect of SWNHs on cancer cells than normal (Figure 2H).

Cells were mixed with BrdU to investigate the effect of SWNHs on mitosis entry. Our results indicated that mitotic entry of both cells was delayed noticeably by SWNHs (Figure 3A and B) and that proliferation of cells was suppressed (Figure 3C,D) in a concentration- and time-dependent manner (P<0.01). The role was more significant in HepG2 than in L02.

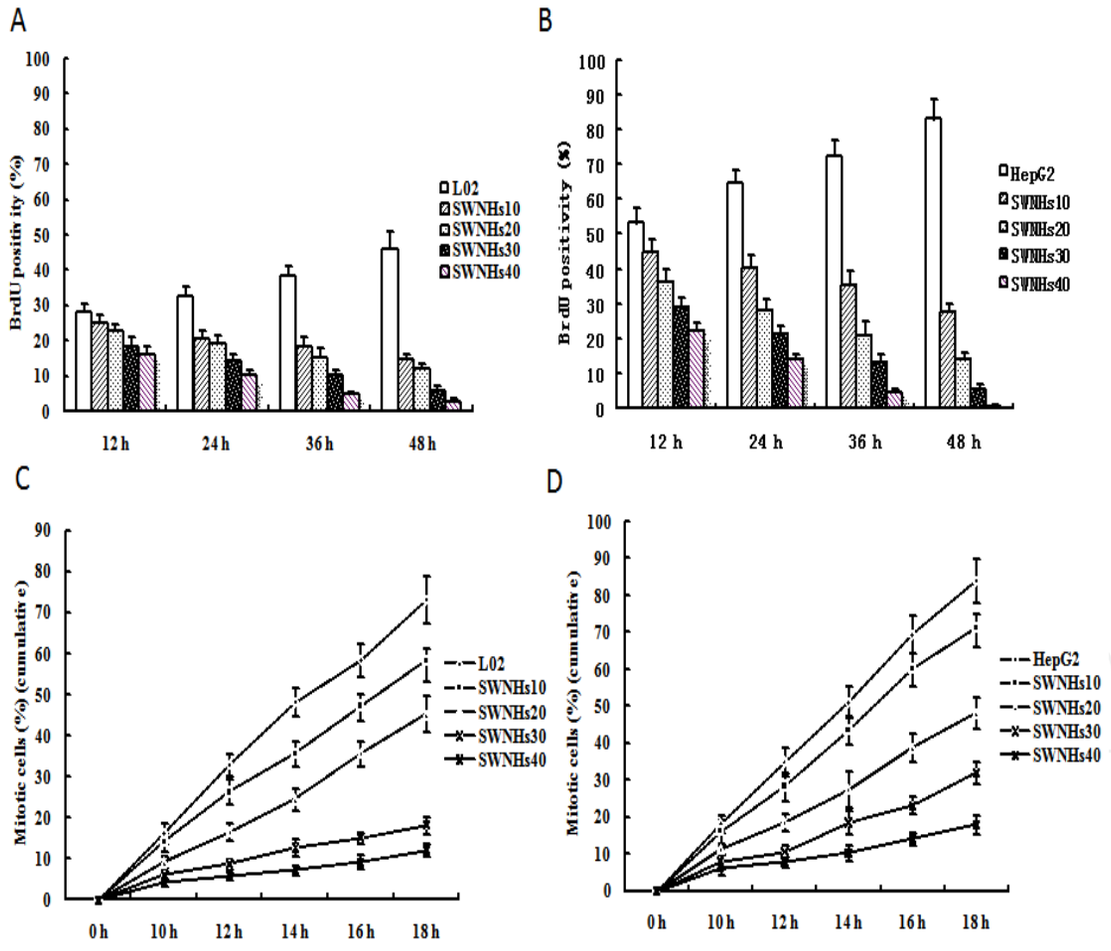


Figure 3. SWNHs inhibited mitotic entry of liver cells. L02 (3×10^5) and HepG2 (3×10^5) cells were seeded onto 60-mm Non- and SWNHs-coated dishes, and cultured for 48 h. To assure how the SWNHs affect cellular mitosis, we incorporated BrdU into the control, and found that accumulations of both mitotic L02 (A) and HepG2 (B) cells were significantly delayed and their mitotic entry (C,D) was inhibited by SWNHs at every time point followed with the increasing quantities of SWNHs (P<0.01). All data are represented as mean ±SEM.

http://dx.doi.org/10.5772/61109

The results of XTT assay suggested that HepG2 and L02 cells (Figure 4) all were noticeably inhibited in a concentration- and time-dependent manner (P<0.001). The cell viability was valued by the CCK-8 assay, and these results demonstrated that cell proliferation of HepG2 and L02 cells (Figure 4) was inhibited by SWNHs in a concentration- and time-dependent manner (P<0.001).

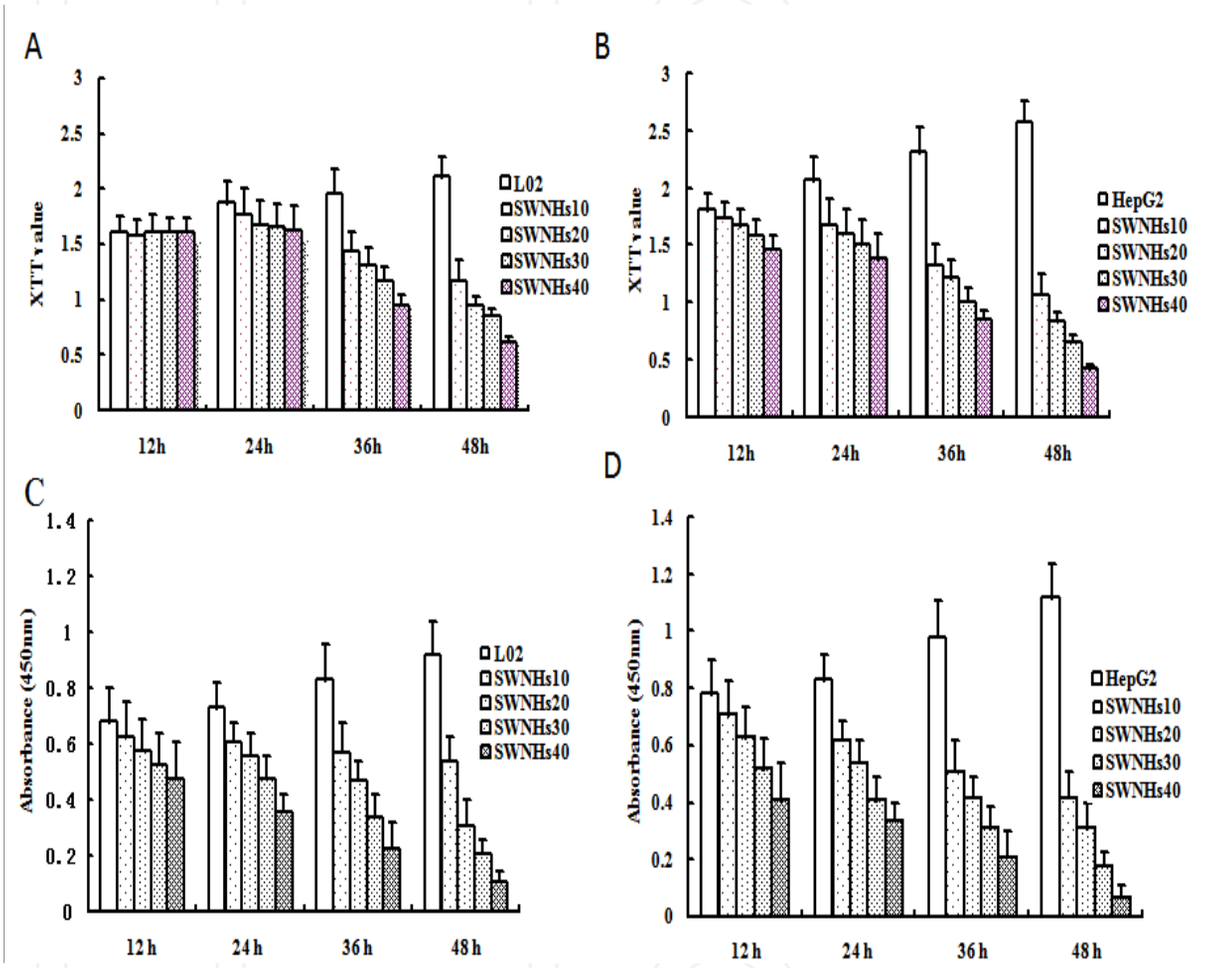


Figure 4. SWNHs inhibited growth and proliferation of liver cells. L02 (3×10^5) and HepG2 (3×10^5) cells were seeded onto 60-mm non- and SWNHs-coated dishes, and cultured for 48 h. Then the effects of SWNHs on L02 (Fig. 4A) and HepG2 (Fig. 4B) cells growth were investigated by XTT assays (P<0.001). L02 (Fig. 4C, 3×10^3) and HepG2 (Fig. 4D, 3×10^3) cells were cultured in 96- plate (6-mm) treated with or without SWNHs, then the cell viabilities were evaluated by CCK-8 assay. All data are represented as mean ±SEM.

2.9. Cell cycle affected by SWNHs

Cell cycle affected by SWNHS was detected with flow cytometry. Our results identified that cell cycles of L02 and HepG2 were affected by SWNHs (Figure 5), and in a concentration-dependent manner. The S phase of liver cells noticeably decreased, and the G1 phase increased obviously in a concentration-dependent manner (L02, P<0.05 and HepG2 P<0.01). Furthermore, G2 phase decreased in both cells, but only increased noticeably in HepG2 treated with

SWNHs40 (P<0.05). SWNHs induced different grades of G1 phase delay in HepG2 and L02 cells, which identified different cytotoxic effects on the two cell lines. It led to much stronger suppression of DNA replication in HepG2. The cell cycle was blocked in G2 phase, the gap from DNA synthesis to mitosis was delayed by SWNHs40 in HepG2, which induced apoptosis of HepG2 cells. [27]

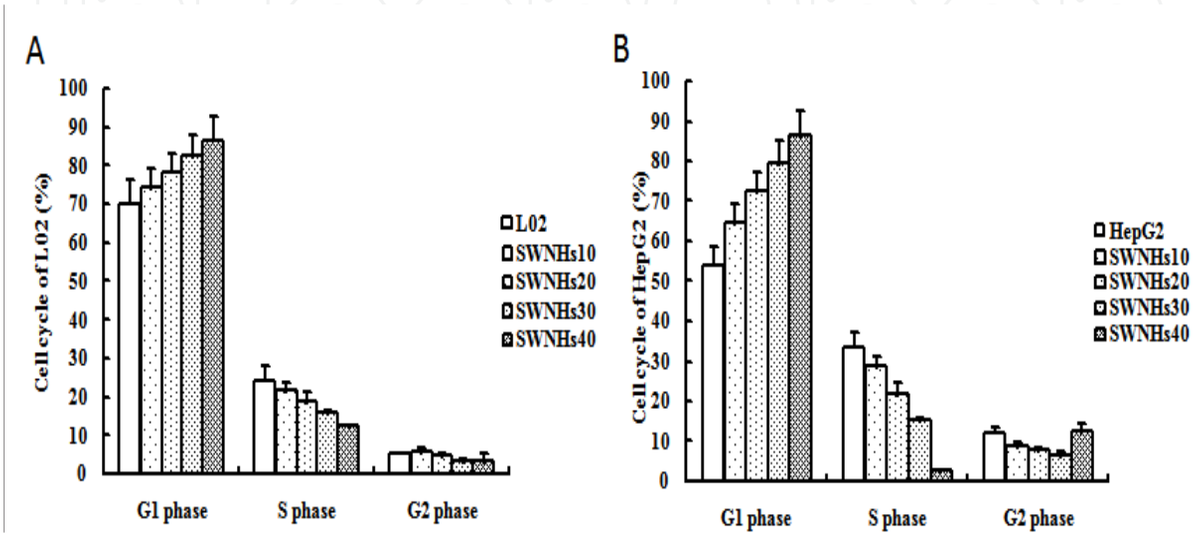


Figure 5. SWNHs affected cell cycle of liver cells. L02 (3×10^5) and HepG2 (3×10^5) cells were seeded onto non- and SWNHs-coated 60mm-dishes, and cultured for 48 h, respectively. Then the roles of SWNHs on L02 (A) and HepG2 (B) cell cycles were measured by cytometry. All data are represented as mean ±S.E.M.

2.10. SWNHs induced apoptosis

The apoptotic cells were determined by 7-AAD and Annexin-V. Our results indicated that apoptosis of HepG2 and L02 (Figure 6) were caused by SWNHs in a concentration-dependent manner, especially in HepG2 (P<0.001).

Biochemical events of apoptosis induce characteristic changes and death of cells. These changes include chromosomal DNA fragmentation, chromatin condensation, nuclear fragmentation, cell shrinkage and blebbing. Apoptosis in mammalian animal cells is regulated by SIRT1 and p53. Caspases are a group of cysteine proteases, and the key factors in cell apoptosis, such as caspase-3 and caspase-7. Our results identified that the expression of p53, caspase-7, and caspase-3 increased in L02 and HepG2 (Figure 6) in a concentration-dependent manner. Moreover, activation cleavage SIRT1 expression decreased in a dose-dependent manner. It confirmed that apoptosis of liver cells was promoted by SWNHs.

2.11. Cellular morphology observed by confocal microscope

The confocal images showed the morphology of L02; cell shapes of their nuclei were similar to control (Figure 7A), and number of cells decreased in a concentration-dependent manner.

http://dx.doi.org/10.5772/61109

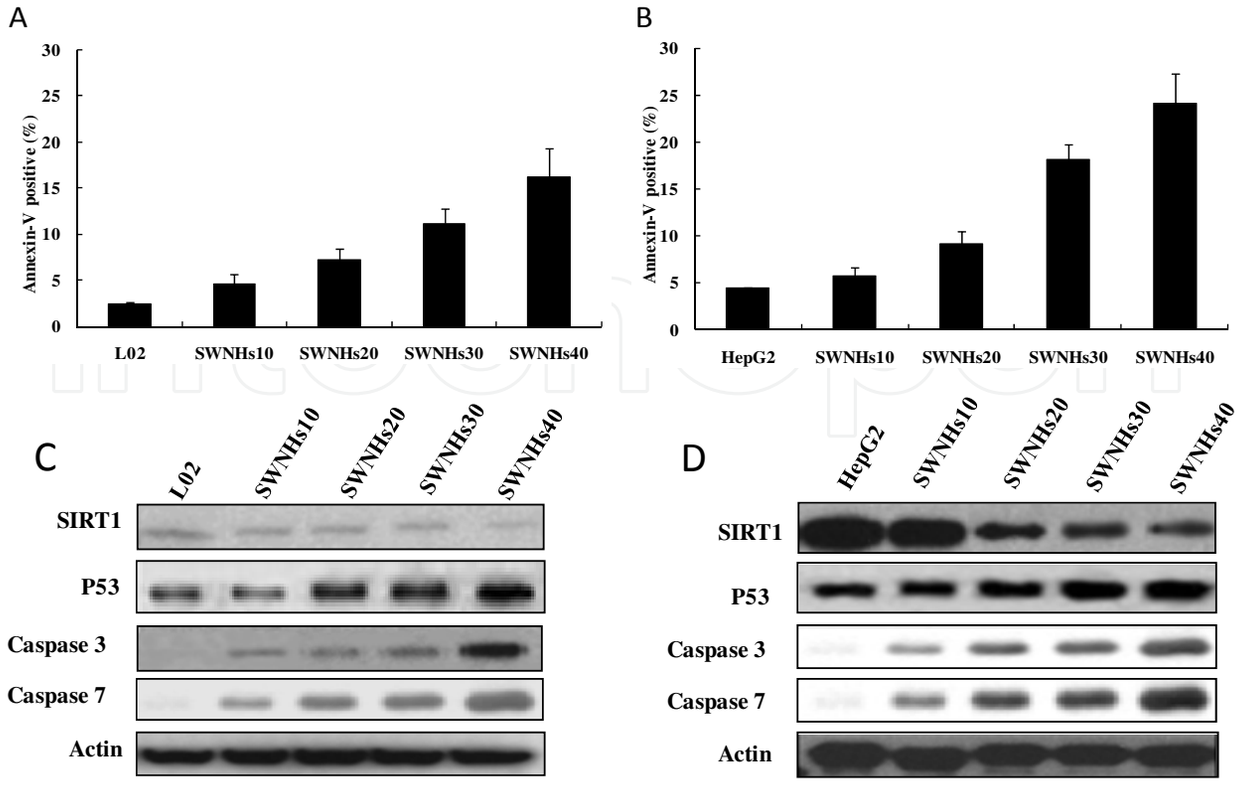


Figure 6. SWNHs promoted cell apoptosis of liver cells and apoptosis involves key factors in vivo. L02 (3×10^5) and HepG2 (3×10^5) Cells were seeded onto 60-mm non- and SWNHs-coated PS dishes, and cultured for 48 h, respectively. Then the effect of SWNHs on L02 (A) and HepG2 (B) cell apoptosis distribution was determined by flow cytometry (P=0.001). The expression levels of SIRT1 and those of activation cleavage of P53, caspase-3 and caspase-7 L02 (C) and HepG2 (D) were determined by western blotting. All data are represented as mean ±S.E.M.

In L02 treated with SWNHs, the size of nuclei was slightly larger than control (Figure 7B,C); the nuclei swelled following the increasing of SWNHs concentration.

The number of viable HepG2 decreased remarkably and apoptotic HepG2 increased in a concentration-dependent manner. Apoptotic HepG2 cells could be found in Figure 7F (showed as arrow), but could not be observed in controls (Figure 7D).

The images of HepG2 treated with SWNHs40 indicated that the size of nuclei was much smaller than control. As reported by Romero et al., [23] karyopyknosis was induced by SWNHs (Figure 7 F, showed as arrows). The karyopyknosis and larger nuclei caused by SWNHs were benefit of increased protein content of earlier apoptosis and decreased content of late apoptosis in nuclei. It may elucidate the suddenly increased G2 phase in HepG2 cells deal with SWNHs 40 (Figure5B). HepG2 cells deal with SWNHs 40 was nearly all apoptotic, meanwhile the ratio of S phase decreased remarkably and cells were obstructed at the G2/M phase. But, few L02 cells were apoptosis effects induced by SWNHs. HepG2 deal with SWNHs40 illustrated classic apoptotic morphology, but there were not so obvious apoptotic L02 cells. The apoptotic cells showed typical features, such as cell shrinkage, chromatin condensation, membrane blebbing, scant cytoplasm, and apoptotic body, [43, 45] especially in HepG2 cells.

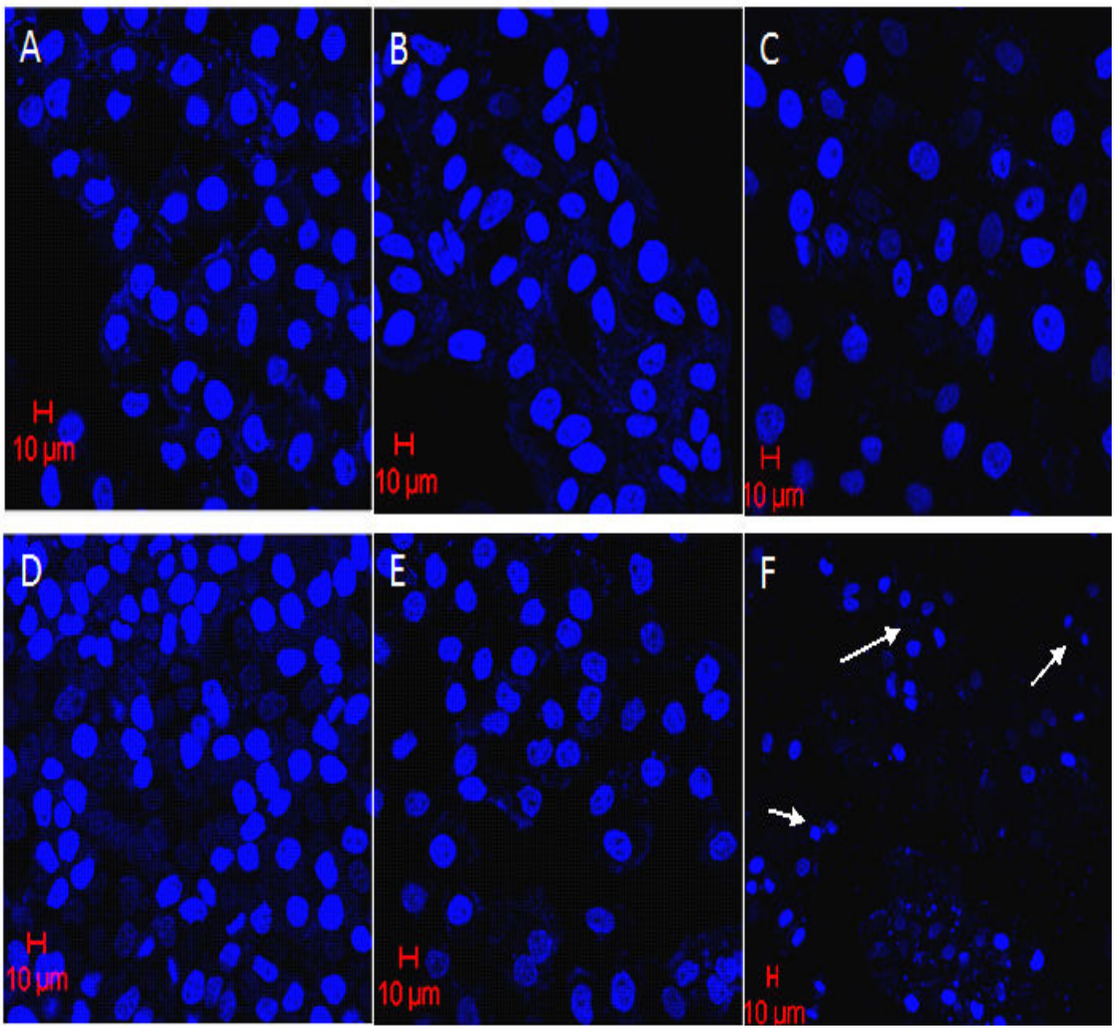


Figure 7. Morphology of L02 and HepG2 cells cultured onto SWNHs-coated dishes observed by confocalmicroscope. L02 (1×10^4) and HepG2 (1×10^4) cells were seeded onto 10-mm non- and SWNHs-coated dishes, and cultured in DMEM with FBS and PSN at 37 °C in humidified 5% CO_2/95% air for 48 h, respectively. Then L02 and HepG2 cells were treated with PFA and DAPI, and confocal images were acquired by Zeiss 510 META confocal microscope. (A) Control, L02 untreated with SWNHs; (B) L02 treated with SWNHs20 (0.42ìg/cm^2); (C) L02 treated with SWNHs40 (0.85ìg/cm^2) (D) Control, HepG2 untreated with SWNHs; (E) HepG2 treated with SWNHs20 (0.42ìg/cm^2). (F) HepG2 treated with SWNHs40 (0.85ìg/cm^2). Scale bars represent 10 ìm.

2.12. TEM

Cells deal with SWNHs40 (0.85 μg/cm^2) were collected for Transmission Electron Microscopy (TEM) measurement. By TEM, SWNHs can be found in cells. In L02, SWNHs aggregate localized at lysosomes and was smaller than 100 nm (Figure 8B and C). Moreover, it localized at nuclei in HepG2 cells (Figure 8E and F). The individual particles of SWNHs were easily dispersed from their neighbor molecules based on SWNHs possess high electronic densities on the surface than other molecules in organelles. The TEM images of organelles showed that both lysosomes and mitochondria in L02 (Figure8G) and HepG2 (Figure8H) deal with SWNHs were larger than control, respectively. And it was more remarkable in HepG2. Outside L02

(Figure8G) and HepG2 cells (Figure8H) deal with SWNHs, there were a lot of secretory vesicles, but not seen outside control cells. The secretory vesicles outside HepG2 (Figure8H) deal with SWNHs were larger than those outside L02 (Figure8G). SWNHs were heterogeneous materials, so cells secreted ingested SWNHs as normal response. HepG2 may have ingested much more SWNHs than L02. And the more cells ingested SWNHs, the more there were secretory vesicles.

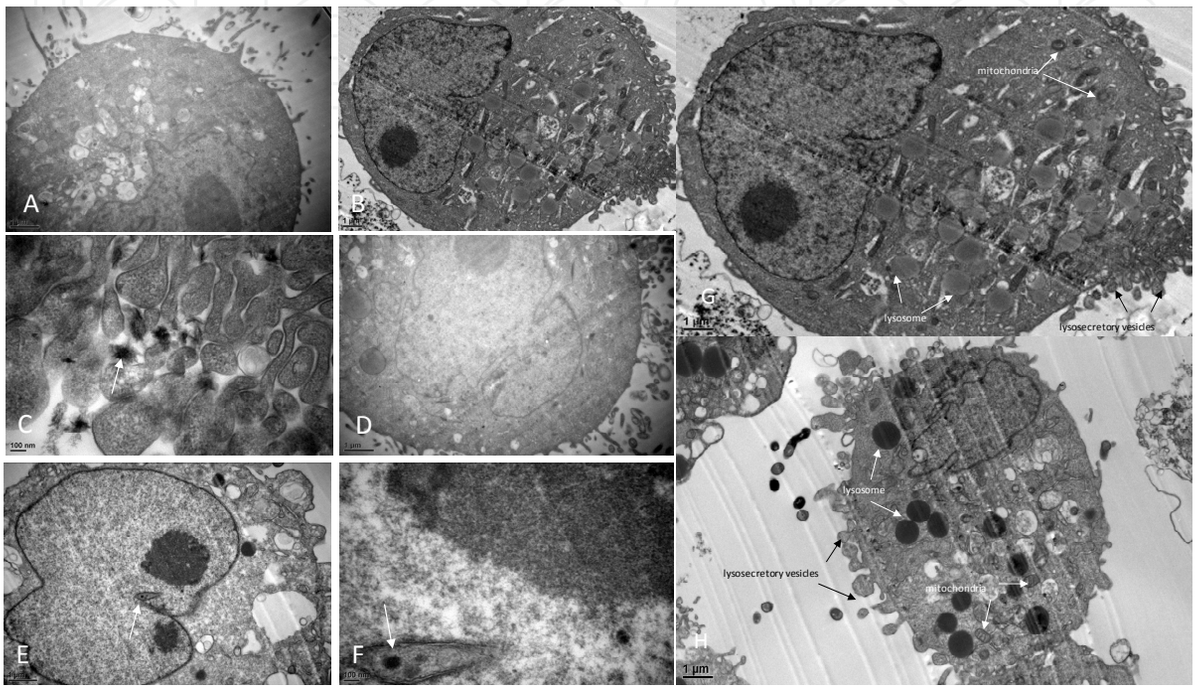


Figure 8. TEM images of liver cells. L02 (3×10^5) and HepG2 (3×10^5) Cells were seeded onto 60-mm non- and SWNHs40-coated (0.85 ìg/cm^2) dishes, and cultured for 48 h, respectively. The cells were collected and fixed with 3% glutaraldehyde. For TEM, ultrathin cells slices of 100 nm thickness were cut using an ultramicrotome and mounted on grids. The slices were contrasted with aqueous solution of uranyl acetate and lead citrate, and examined on JEM-1400 Transmission Electron Microscope (JEOL Ltd, Japan) with accelerating voltage of 80 kV. (A) L02 untreated with SWNHs as control (15,000×). Scale bar represents 1 ìm. (B) L02 cultured onto SWNHs40-coated dishes (0.85 ìg/cm^2) for 48 h (15,000×). Scale bar represents 1 ìm. (C) L02 cultured onto SWNHs40-coated dishes (0.85 ìg/cm^2) for 48 h (80,000×). Scale bar represents 100 nm. The arrow in Fig. 8B and Fig. 8C showed that there were individual spherical SWNHs particles with diameter less than 100 nm inside lysosomes of L02 cells. (D) HepG2 untreated with SWNHs as control (15,000×). Scale bar represents 1 ìm. (E) HepG2 cultured onto SWNHs40-coated dishes (0.85 ìg/cm^2) for 48 h (15,000×). Scale bar represents 1 ìm. (F) HepG2 cultured onto SWNHs40-coated dishes (0.85 ìg/cm^2) for 48 h (80,000×). Scale bar represents 100 nm. The arrow in Fig. 8E and Fig. 8F showed that there were individual spherical SWNHs particles with diameters less than 100 nm inside nuclei of HepG2 cells. (G) L02 cultured onto SWNHs40-coated dishes (0.85 ìg/cm^2) for 48 h (15,000×). Scale bar represents 1 ìm. (H) HepG2 cells cultured onto SWNHs40-coated dishes (0.85 ìg/cm^2) for 48 h (15,000×). Scale bar represents 1 ìm.

3. Discussion

The aforementioned studies have illustrated that some carbon nanomaterials suppressed growth and proliferation of L02 or HepG2. Fullerene C60 inhibited proliferation of HepG2 at

a low dosage of 0.46 μg/mL. [30]Liu et al. [29]suggested that unmodified MWNTs (multiwalled nanotubes), MWNTs modified with carboxyl, and MWNTs modified with hydroxyl at dosages of 12.5–200.0 μg/mL inhibited viability of L02 cells in a dose-dependent manner. Romero et al. [23] illustrated that poly [sulfopropyl methacrylate] (PSPM), or oxidized, lipid, poly [allylamine hydrochloride] (PAH)-modified MWNTs at higher dosage (100 μg/mL) suppressed growth and proliferation of HepG2. It was well known that SWCNTs (single-walled carbon nanotubes) had great potential to benefit biomedicine, for example, photothermal ablation therapy for tumor bond with near-infrared irradiation. Hashida et al. [46] reported the photothermal activity of a novel SWCNT bond with (KFKA) 7 peptide [H-(-Lys-Phe-Lys-Ala-)7-OH] with repeated structure, which could be used to treat tumor. The SWCNTs–(KFKA) 7 compounds could be used to ablate tumor in photothermal cancer therapy with its high aqueous dispersibility. [46] Our results were similar in HepG2 and L02 cells deal with SWNHs at low dose (1.5–6.0 μg/mL). Ajima et al. [4] reported that SWNHox (oxidized SWNHs) did not suppress or promote proliferation of lung cancer cells at dose of 0–20 μg/mL. But *in vivo*, their results indicated that SWNHox itself could be used to treat cancer, contrary to results from *in vitro* experiments. [7] Fan et al. [8] identified that there was no significant decrease in cell viability in Hela cells treated with SWNHs modified with gum Arabic (10–1000 μg/mL). These results illustrated that these nanoparticles were nontoxic to the cells. Tahara et al. [9] found recently that oxidized SWNHs coated with 1, 2-distearoyl-Sn-glycero-3-phosphoethanolamine-N- [amino (polyethylene, glycol) 2000] could suppress the growth and proliferation of murine macrophage RAW 264.7 cells in a concentration-dependent manner. The different modification styles for carbon nonmaterial based on different chemical compounds may induce change of various biological functions in different cells. [43]

After exposure to a chemical toxicant, the most easily and first visualized change and effect in cells could be observed come from cell morphology. So, morphological changes were benefit for toxicity biomarker. TEM could be used to identify the location of nanoparticles in organelles of cells based on its powerful denote to observing micron and nanometer structures. Oxidized SWNTs or modified and unmodified MWNTs could be found in endosomes, cytoplasm, or lysosomes of human macrophage cells by TEM. [19, 20] Porter et al. [18] found that dispersed SWNTs in tetrahydrofuran localized in nuclei and lysosomes of human macrophages. And fullerene C_{60} could be found in nuclei and cytoplasm of human macrophages. [47] Besides in endosomes, cytoplasm, or lysosomes, in human embryonic kidney 293 cells, MWNT-NH2 was first found in nuclei. [21] In HepG2 cells, the PSPM, lipid, or oxidized-modified MWNTs could be discovered in cytoplasm. However, there were no references involved in carbon nanoparticles locating in the nuclei of cells. Although, in nuclei of HepG2 cells, changes of protein and DNA had been obtained based on confocal Raman microscope induced by modified MWNTs. [23] Combining the results from TEM and confocal microscope, we identified the different interactive mechanisms between SWNHs and L02 or HepG2 cells, respectively. SWNHs could directly enter into nuclei of HepG2 and could induce cell apoptosis, while SWNHs could induce apoptosis of L02 cells associated with activation of lysosomal function.

Changes in growth of cells also could be determined as a toxic effect. The chemical toxicities could be assessed by an assay called plating efficiency. This evaluated the ability of cells to form colonies after 15 days of culture in the presence of a substance, signaling cell survival and ability to reproduce. Another assay that evaluated the capability of cells to replicate and

http://dx.doi.org/10.5772/61109

determined the concentration of the substance at which 50% of the cells do not multiply is named the median inhibitory dose (ID50). Romero et al. [23] illustrated the effects of inhibiting role on cell proliferation caused by apoptosis, which as toxicity of carbon nanotubes (CNTs) for HepG2 *in vitro*. Moreover, cytotoxicity for cancer cells may have potential therapeutic value. Our results indicated that SWNHs had larger toxicity in HepG2 cells than in L02. In different cells, this major difference may be based on SWNHs surface structure selective affinity to subcellular structures. Based on these differences, new drug carriers or drugs with special structures of SWNHs may be planned for clinical pharmaceutical therapy, especially cancer photothermal therapy. [48 50] According to the affinity to nuclei in HepG2, the scene of designing cell-targeted drugs might be considered to SWNHs.

In fact, SWNHs themselves suppressed growth and proliferation of HepG2 cells; meanwhile induced their apoptosis. It revealed that SWNHs material could be used as a drug carrier for anti-HCC, and carried anticancer drugs such as cisplatin based on its cooperative therapeutic role.

Nanoparticle almost all located in lysosome and was degradated and sequestrated. The mitochondrial apoptosis and lysosomal dysfunctions could induce toxicological consequences. [51, 52] Based on oxidative stress pathway related to apoptosis caused by nanoparticle, [33] localization of nanoparticles may induce activation of lysosome, which with high content of digestive enzyme, triggering mitochondrial apoptosis. [34] Mitochondria was the main basis of redox and ROS (reactive oxygen species) machinery in cells, and could activate inflammatory cytokines. [32] Oxidative stress toke place in HepG2 cells deal with oxidized or unmodified MWNTs and SWNTs, [25, 28] and in L02 cells deal with hydroxyl-modified, carboxyl-modified or unmodified MWNTs, [29] and in rat hepatocytes deal with fullerenes $C_{60}(OH)_{24}$, $C_{60}(OH)_{12}$, and C_{60}. [31] Gao et al. [19] found that modified MWNTs internalized into human macrophages cells THP-1 and located in lysosomes, induced ROG generation and low mitochondrial membrane potential. Tahara et al. [9] identified that high concentration of SWNHs caused destabilization of lysosomal membrane and ROS generation in murine macrophage RAW 264.7. The results of us demonstrated individual SWNH particles located at mitochondria of L02 and HepG2, or lysosomes of L02 cells. It suggested that mitochondrial apoptosis and lysosomal dysfunctions in liver cells play key role on physiological process related to SWNHs exposure.

The model of transmembrane pathways divided MWNTs into two classes types, singles and clusters. The clusters of CNT were collected in cells associated with energy-dependent endocytosis process; meanwhile extremely dispersed single CNTs directly penetrated cellular membranes entried into cells. [2, 1] We will assure the transmembrane pathway of SWNHs. Because one spherical SWNH aggregate were assembled by about 2000 nanohorns, the aggregates showed clusters of SWNHs. [9] Nevertheless, the aggregate more like one single nanoparticle, and not easy to separate into individual nanohorns. Porter et al. [1, 8] identified the internalization of SWNTs with smaller diameters of SWNTs (0.6–3.5 nm) in cells through nuclear pore complex and other pores. [18] A single SWNHs aggregate has larger diameter (60–100 nm) than fullerene C_{60} (0.7 nm) and single SWNTs (0.6–3.5 nm). It is very interesting how aggregates of individual spherical SWNH composed with 2000 nanohorns internalize in cells and localize at lysosomes in L02 cells, and even entry into the nuclei of HepG2 cells.

Because it was suggested that only nanoparticles less than 40 nm in diameter could enter into nuclei of cells. [53] The low negative charge density on surfaces of SWNHs and the bovine serum proteins used in cell culture may be benefit for SWNH dispersion in culture media, or induce SWNHs recognized with cellular membranes by receptors on the surface of cells. [54]

Researches in this area remain many questions. How SWNHs enter into different cells and locate at different destinations (such as nuclei, liposome, or mitochondria) in different cells? How SWNHs induce the apoptosis in different cells? However, toxicity is a complex event showing several effects, even cell death until metabolic aberrations. Neuro-, liver, and/or kidney toxicity are examples of functional changes not necessarily events linked to cell death. Due to these evidences, the *in vitro* cytotoxicity assays need to exploit different parameters in the cell biochemistry. The assays are important tools to amplify the knowledge about the cytotoxic effects triggered by chemical substances and to predict the toxicity in humans.

Nanotoxicology examines the bioeffects of nanomaterials concerning the toxic activities and depends on the *in vitro* system investigated. Then, validation of *in vitro* assays will be valuable for safety or hazard investigation in an analysis against standard nanostructures. The cell-based toxicity assays can be used to assess potential safety use in the investigation of new potential drugs and to study the correlation between structure, toxicity, and biological activity, permitting changes in the structure chemical or in the formulation with the aim to improve drug-like properties.

The cell culture assays have as advantages the fast results in the research, reduced cost, and a few quantities of substance to be used. Besides that, those models can predict toxicity in animals including humans to get more precise results to establish multitiered *in vitro* screening models.

In this way, the primary goal of *in vitro* models in the toxicity evaluation could be to predict the toxicity *in vivo*, especially human toxicity. The screening permits investigation of the metabolism and biochemical reactions of different substances in order to obtain knowledge about the pharmacokinetics and bioavailability of the drugs. Studies about bioavailability, chemical and metabolic stability, and permeability are necessary *in vitro* screening models that help predicting the human toxicity.

Author details

Guoan Xiang[1*], Jinqian Zhang[2] and Rui Huang[1]

*Address all correspondence to: guoan_66@163.com

1 Department of General Surgery, The Second People's Hospital of Guangdong Province, Southern Medical University, Guangzhou, People's Republic of China

2 Research Center, The Second People's Hospital of Guangdong Province, Southern Medical University, Beijing, People's Republic of China

http://dx.doi.org/10.5772/61109

References

[1] Iijima S, Yudasaka M, Yamada R, et al. Nano aggregates of single-walled graphitic carbon nano-horns. *Chem Phys Lett*. 1999;309(3):165–170.

[2] Murakami T, Tsuchida K. Recent advances in inorganic nanoparticle-based drug delivery systems. *Mini Rev Med Chem*. 2008;8(2):175–183.

[3] Xu JX, Yudasaka M, Kouraba S, Sekido M, Yamamoto Y, Iijima S. Single-wall carbon nanohorn as a drug carrier for controlled release. *Chem Phys Lett*. 2008;461(4–6):189–192.

[4] Ajima K, Yudasaka M, Murakami T, Maigné A, Shiba K, Iijima S. Carbon nanohorns as anticancer drug carriers. *Mol Pharm*. 2005;2(6): 475–480.

[5] Matsumura S, Ajima K, Yudasaka M, Iijima S, Shiba K. Dispersion of cisplatin-loaded carbon nanohorns with a conjugate comprised of an artificial peptide aptamer and polyethylene glycol. *Mol Pharm*. 2007;4(5): 723–729.

[6] Murakami T, Sawada H, Tamura G, Yudasaka M, Iijima S, Tsuchida K. Water-dispersed single-wall carbon nanohorns as drug carriers for local cancer chemotherapy. *Nanomedicine (Lond)*. 2008;3(4):453–463.

[7] Ajima K, Murakami T, Mizoguchi Y, et al. Enhancement of in vivo anticancer effects of cisplatin by incorporation inside single-wall carbon nanohorns. *ACS Nano*. 2008;2(10):2057–2064.

[8] Fan XB, Tan J, Zhang GL, Zhang FB. Isolation of carbon nanohorn assemblies and their potential for intracellular delivery. *Nanotechnology*. 2007;18(19):195103–195108.

[9] Tahara Y, Nakamura M, Yang M, Zhang M, Iijima S, Yudasaka M. Lysosomal membrane destabilization induced by high accumulation of single-walled carbon nanohorns in murine macrophage RAW 264.7. *Biomaterials*. 2012;33(9):2762–2769.

[10] Akasaka T, Yokoyama A, Matsuoka M, Hashimoto T, Watari F. Thin films of single-walled carbon nanotubes promote human osteoblastic cells (Saos-2) proliferation in low serum concentrations. *Mater Sci Eng C*. 2010;30(3):391–399.

[11] Nayak TR, Jian L, Phua LC, Ho HK, Ren Y, Pastorin G. Thin films of functionalized multiwalled carbon nanotubes as suitablescaffold materials for stem cells proliferation and bone formation. *ACS Nano*. 2010;4(12):7717–7725.

[12] Namgung S, Baik KY, Park J, Hong S. Controlling the growth and differentiation of human mesenchymal stem cells by the arrangement of individual carbon nanotubes. *ACS Nano*. 2011;5(9):7383–7390.

[13] Davoren M, Herzog E, Casey A, et al. In vitro toxicity evaluation of single walled carbon nanotubes on human A549 lung cells. *Toxicol In Vitro*. 2007;21(3):438–448.

[14] Albini A, Mussi V, Parodi A, et al. Interactions of single-wall carbon nanotubes with endothelial cells. *Nanomedicine*. 2010;6(2):277–288.

[15] Cheng C, Porter AE, Muller K, et al. Imaging carbon nanoparticles and related cytotoxicity. *J Phys Conf Ser*. 2009;151(1):012030.

[16] Neves V, Gerondopoulos A, Heister E, et al. Cellular localization, accumulation and trafficking of double-walled carbon nanotubes in human prostate cancer cells. *Nano Res*. 2012;5(4):223–234.

[17] Di Giorgio ML, Di Bucchianico S, Ragnelli AM, Aimola P, Santucci S, Poma A. Effects of single and multi walled carbon nanotubes on macrophages: cyto and genotoxicity and electron microscopy. *Mutat Res*. 2011;722(1):20–31.

[18] Porter AE, Gass M, Muller K, Skepper JN, Midgley PA, Welland M. Direct imaging of single-walled carbon nanotubes in cells. *Nat Nanotechnol*. 2007;2(11):713–717.

[19] Gao N, Zhang Q, Mu Q, et al. Steering carbon nanotubes to scavenger receptor recognition by nanotube surface chemistry modification partially alleviates NFκB activation and reduces its immunotoxicity. *ACS Nano*. 2011;5(6):4581–4591.

[20] Porter AE, Gass M, Bendall JS, et al. Uptake of noncytotoxic acid treated single-walled carbon nanotubes into the cytoplasm of human macrophage cells. *ACS Nano*. 2009;3(6):1485–1492.

[21] Mu Q, Broughton DL, Yan B. Endosomal leakage and nuclear translocation of multiwalled carbon nanotubes: developing a model for cell uptake. *Nano Lett*. 2009;9(12): 4370–4375.

[22] Zhou F, Xing D, Wu B, Wu S, Ou Z, Chen WR. New insights of transmembranal mechanism and subcellular localization of noncovalently modified single-walled carbon nanotubes. *Nano Lett*. 2010;10(5): 1677–1681.

[23] Romero G, Estrela-Lopis I, Castro-Hartmann P, et al. Stepwise surface tailoring of carbon nanotubes with polyelectrolyte brushes and lipid layers to control their intracellular distribution and 'in vitro' toxicity. *Soft Matter*. 2011;7(15):6883–6890.

[24] Li L, Zhang J, Yang Y, et al. Single-wall carbon nanohorns inhibited activation of microglia induced by lipopolysaccharide through blocking of Sirt3. *Nanoscale Res Lett*. 2013;8(1):100.

[25] Piret JP, Vankoningsloo S, Noël F, et al. Inflammation response at the transcriptional level of HepG2 cells induced by multi-walled carbon nanotubes. *J Phys Conf Ser*. 2011;304(1):012040.

[26] Yuan J, Gao H, Sui J, Chen WN, Ching CB. Cytotoxicity of singlewalled carbon nanotubes on human hepatoma HepG2 cells: an iTRAQcoupled 2D LC-MS/MS proteome analysis. *Toxicol In Vitro*. 2011; 25(8):1820–1827.

[27] Yuan J, Gao H, Sui J, Duan H, Chen WN, Ching CB. Cytotoxicity evaluation of oxidized single-walled carbon nanotubes and graphene oxide on human hepatoma

HepG2 cells: an iTRAQ-coupled 2D LC-MS/MS proteome analysis. *Toxicol Sci*. 2012;126(1):149–161.

[28] Yuan J, Gao H, Ching CB. Comparative protein profile of human hepatoma HepG2 cells treated with graphene and single-walled carbon nanotubes: an iTRAQ-coupled 2D LC-MS/MS proteome analysis. *Toxicol Lett*. 2011;207(3):213–221.

[29] Liu ZB, Zhou B, Wang HY, et al. Effect of functionalized multi-walled carbon nanotubes on L02 cells. *Acta Academiae Medicinae Sinicae*. (Chinese) 2010;32(4):449–455.

[30] Matsuda S, Matsui S, Shimizu Y, Matsuda T. Genotoxicity of colloidal fullerene C60. *Environ Sci Technol*. 2011;45(9):4133–4138.

[31] Nakagawa Y, Suzuki T, Ishii H, Nakae D, Ogata A. Cytotoxic effects of hydroxylated fullerenes on isolated rat hepatocytes via mitochondrial dysfunction. *Arch Toxicol*. 2011;85(11):1429–1440.

[32] Wang X, Xia T, Duch MC, et al. Pluronic F108 coating decreases the lung fibrosis potential of multiwall carbon nanotubes by reducing lysosomal injury. *Nano Lett*. 2012;12(6):3050–3061.

[33] Shvedova AA, Pietroiusti A, Fadeel B, Kagan VE. Mechanisms of carbon nanotube-induced toxicity: focus on oxidative stress. *Toxicol Appl Pharmacol*. 2012;261(2):121–133.

[34] Andón FT, Fadeel B. Programmed cell death: molecular mechanisms and implications for safety assessment of nanomaterials. *Acc Chem Res*. 2013;46(3):733–742.

[35] Wei L, Lu N, Dai Q, et al. Different apoptotic effects of wogonin via induction of H(2)O(2) generation and Ca(2+) overload in malignant hepatoma and normal hepatic cells. *J Cell Biochem*. 2010;111(6): 1629–1641.

[36] Das SK, Hashimoto T, Kanazawa K. Growth inhibition of human hepatic carcinoma HepG2 cells by fucoxanthin is associated with down-regulation of cyclin D. *Biochim Biophys Acta*. 2008;1780(4):743–749.

[37] Li N, Wang Z, Zhao K, Shi Z, Gu Z, Xu S. Synthesis of single-wall carbon nanohorns by arc-discharge in air and their formation mechanism. *Carbon*. 2010;48(5):1580–1585.

[38] Jiang H, Wu J, He C, Yang W, Li H. Tumor suppressor protein C53 antagonizes checkpoint kinases to promote cyclin-dependent kinase 1 activation. *Cell Res*. 2009;19(4):458–468.

[39] Ford J, Jiang M, Milner J. Cancer-specific functions of SIRT1 enable human epithelial cancer cell growth and survival. *Cancer Res*. 2005; 65(22):10457–10463.

[40] Hamamoto R, Furukawa Y, Morita M, et al. SMYD3 encodes a histone methyltransferase involved in the proliferation of cancer cells. *Nat Cell Biol*. 2004;6(8):731–740.

[41] Li H, Bergeron L, Cryns V, et al. Activation of caspase-2 in apoptosis. *J Biol Chem*. 1997;272(34):21010–21017.

[42] Murata K, Kaneko K, Kokai F, Takahashi K, Yudasaka M, Iijima S. Pore structure of single-wall carbon nanohorn aggregates. *Chem Phys Lett*. 2000;331(1):14–20.

[43] Sohaebuddin SK, Thevenot PT, Baker D, Eaton JW, Tang L. Nanomaterial cytotoxicity is composition, size, and cell type dependent. *Part Fibre Toxicol*. 2010;7:22.

[44] Stewart MS, Davis RL, Walsh LP, Pence BC. Induction of differentiation and apoptosis by sodium selenite in human colonic carcinoma cells (HT29). *Cancer Lett*. 1997;117(1):35–40.

[45] Edinger AL, Thompson CB. Death by design: apoptosis, necrosis and autophagy. *Curr Opin Cell Biol*. 2004;16(6):663–669.

[46] Hashida Y, Tanaka H, Zhou S, et al. Photothermal ablation of tumor cells using a single-walled carbon nanotube-peptide composite. *J Control Release*. 2013;173C:59–66.

[47] Porter AE, Gass M, Muller K, Skepper JN, Midgley P, Welland M. Visualizing the uptake of C60 to the cytoplasm and nucleus of human monocyte-derived macrophage cells using energy-filtered transmission electron microscopy and electron tomography. *Environ Sci Technol*. 2007;41(8):3012–3017.

[48] Iancu C, Mocan L, Bele C, et al. Enhanced laser thermal ablation for the in vitro treatment of liver cancer by specific delivery of multiwalled carbon nanotubes functionalized with human serum albumin. *Int J Nanomedicine*. 2011;6:129–141.

[49] Lei HY, Peng CA, Tang MJ, Reindhart K, Szu HH. Con_A-carbone nanotube conjugate with short wave near-infrared laser ablation for tumor therapy. *Proc SPIE*. 2009;7343:73430Q.

[50] Zhou F, Xing D, Chen WR. Direct imaging the subcellular localization of single-walled carbon nanotubes. *Proc SPIE*. 2011;7900:79000E.

[51] Stern ST, Adiseshaiah PP, Crist RM. Autophagy and lysosomal dysfunction as emerging mechanisms of nanomaterial toxicity. *Part Fibre Toxicol*. 2012;9:20.

[52] Teodoro JS, Simões AM, Duarte FV, et al. Assessment of the toxicity of silver nanoparticles in vitro: a mitochondrial perspective. *Toxicol In Vitro*. 2011;25(3):664–670.

[53] Dawson KA, Salvati A, Lynch I. Nanotoxicology: nanoparticles reconstruct lipids. *Nat Nanotechnol*. 2009;4(2):84–85.

[54] Fleischer CC, Payne CK. Nanoparticle surface charge mediates the cellular receptors used by protein-nanoparticle complexes. J Phys Chem B. 2012;116(30):8901–8907.